ECS Journal of Solid State Science and Technology, 2025 **14** 116001
2162-8777/2025/14(11)/116001/7/$40.00

A Comparative Analysis of Structural, Microstructural, and Optical Characteristics of Pr^{3+}-Substituted CdS and ZnO Nanoparticles

Jitendra Pal Singh,[1,z] Sudha Pal,[2] Yogesh Kumar Sharma,[3] Atanu Nag,[1] Gulshan Dhillon,[4] Naveen Kumar,[5] and Jyoti Sahu[6]

[1]*Department of Physics, School of Sciences, IFTM University, Moradabad-244102, India*
[2]*Govt. P.G. College, Sitarganj Udham Singh Nagar, Uttrakhand-263139, India*
[3]*Mahayogi Guru Gorakhnath Govt Degree College Bithyani Yamkeshwar (Pauri Garhwal), Uttrakhand-249165, India*
[4]*Department of Applied Sciences, CUIET, Chitkara University, Punjab, India*
[5]*Department of Physics, Galgotias University, Greater Noida, Uttar Pradesh-203201, India*
[6]*Department of Chemical Engineering, N.I.T., Tiruchirapplli, Tamil Nadu-620015, India*

The chemical precipitation method has been utilized to synthesize CdS and ZnO nanoparticles doped with praseodymium ions. The XRD analysis confirmed the structural characteristics of CdS:Pr^{3+} and ZnO:Pr^{3+} nanoparticles. The SEM images validated the size and morphology of the synthesized CdS:Pr^{3+} and ZnO:Pr^{3+} nanoparticles. The nearly spherical and hexagonal shapes observed in the TEM images suggest that the CdS and ZnO nanoparticles predominantly exhibit spherical and hexagonal forms, respectively. Regarding the doping doses, the doped materials' absorption spectra showed a red shift (414–550 nm). Additionally, there is a noticeable absorption of the blue shift. Interestingly, when the radial eigenfunction is believed to be hydrogenic, the calculated ratios of F_4/F_2 and F_6/F_2 are almost the same as those found. All over the Pr^{3+} doping concentration range, the ratio of E^1/E^3 to E^2/E^3 is nearly constant. Applications where improved light absorption throughout a wider spectrum is required, particularly in the field of photo catalysis, Solar cells, and optoelectronics devices, are the main usage for the combined absorption spectra of cadmium sulfide (CdS) and zinc oxide (ZnO).
 [DOI: 10.1149/2162-8777/ae1a18]

Manuscript submitted August 6, 2025; revised manuscript received October 29, 2025. Published November 11, 2025.

Nanoscience is described as the handling of research and development in the range of 1–100 nm. Nanotechnology aims to develop materials with novel properties and functions associated with their small sizes, where the surface area of the small particle is greater. A set of 14 elements with electronic configuration [Xe] $4f^{14}$ $5d^1$ 6s2, with atomic numbers ranging from 57 to 71, appear in the periodic table following lanthanum and are known as rare Earth (RE) ions. In many optical materials, RE ions are crucial components.[1,2] Phosphors used for fluorescent lighting, display monitors, X-ray imaging, scintillators, lasers, and more are only a few of their numerous applications.[3,4] Nanometer-sized particles have low optical scattering, which makes them suitable for their usage as active materials in glass- or polymer-based lasers and amplifiers.

In particular, cadmium sulfide (CdS) nanoparticles (NPs) exhibit unique optical, electrical, and chemical properties, including a wide band gap energy of 2.42 eV at room temperature, making them attractive for optoelectronic, photonic, and photovoltaic applications. However, their luminescence efficiency and stability remain challenges. To address this, RE doping has been employed. Specifically, doping CdS with praseodymium ions (Pr^{3+}) (CdS:Pr^{3+}) introduces localized energy levels that can enhance visible emission and improve device performance. CdSNPs are also widely used as pigments in paints and plastics because of their remarkable thermal stability.[5]

Similarly, zinc oxide (ZnO) nanostructures, including nanowires, nanotubes, nanobelts, and nanorings, are well studied due to their environmentally benign nature, thermal stability, and potential use as blue and ultraviolet light emitters and detectors.[6–10] Yet, their practical applications in field emission displays (FEDs) are limited by insufficient conductivity and reduced emission stability. To overcome this limitation, Pr^{3+} doped ZnO (ZnO:Pr^{3+}) has recently emerged as a strategy to improve conductivity and enhance luminescent efficiency, offering a new pathway for FED phosphor development.[11]

The novelty of the present work lies in the comparative synthesis and investigation of Pr^{3+} doped CdS and ZnONPs, aiming to explore their potential as efficient, stable, and environmentally sustainable phosphors for next-generation optoelectronic and display technologies. According to the aforementioned discussion, Pr^{3+} doped nanocrystalline oxides are exciting candidates for FED phosphor.[12] In this paper, Pr^{3+} doped CdS and ZnONPs were synthesized and their structural and optical properties were systematically studied to demonstrate their suitability as advanced optoelectronics applications.

Experimental

Synthesis.—In this study, CdSNPs were synthesized with simple chemical precipitation method. Cadmium nitrate tetrahydrate, sodium sulphide precursors were used to formulate CdSNPs, which were further employed for the synthesis of CdS:Pr^{3+} NPs. Specifically, 50 ml(0.1 M) of Cadmium Nitrate Tetrahydrate solution [$Cd(NO_3)_2.4H_2O$] was mixed with 20 ml of Diethylene glycol (DEG) under constant stirring. Then, 50 ml of Praseodymium chloride ($PrCl_3$) solution was added drop wise to sodium sulfide solution with continuous stirring. The two solutions were combined, and a yellow precipitate of CdS appeared after maintaining the reaction at 60 °C for 4 h at a pH of ∼10–11. The obtained precipitates were washed with double-distilled water (DDW) and dried at room temperature. The dopant concentration of Pr^{3+} was maintained at 0.1 mol%, 0.2 mol% and 0.3 mol% during synthesis.

For the synthesis of ZnO:Pr^{3+} NPs, 0.272 g of $ZnCl_2$ (0.1 M, 20 ml), 0.545 g NaOH (0.1 M, 100 ml), and glycerol were dissolved separately in ethanol. Glycerol was gradually added to the NaOH solution under constant stirring. After 1 h, $ZnCl_2$ and 0.1 mol%, 0.2 mol% and 0.3 mol% Pr^{3+} solutions were added to the mixture. The reaction was carried out at room temperature (∼25 °C) with pH maintained around 12 for 2 h of stirring, resulting in a milky white colloid. Pr^{3+} doped ZnONPs were obtained as a white powder after washing with ethanol and drying at room temperature. Figure 1 shows the stepwise synthesis procedure of Pr^{3+} doped CdS/ZnONPs.

Characterizations of Pr^{3+} doped CdS/ZnO NPs.—The optical properties of Pr^{3+} doped CdS/ZnO NPs were analyzed using a UV-Visible spectrophotometer. The crystal structure of Pr^{3+} doped CdS/ZnO NPs was determined using PANalyticalX'Pert Pro. The XRD patterns were recorded in reflection mode using Cu K-α radiation

[z]E-mail: paljitendra124@gmail.com

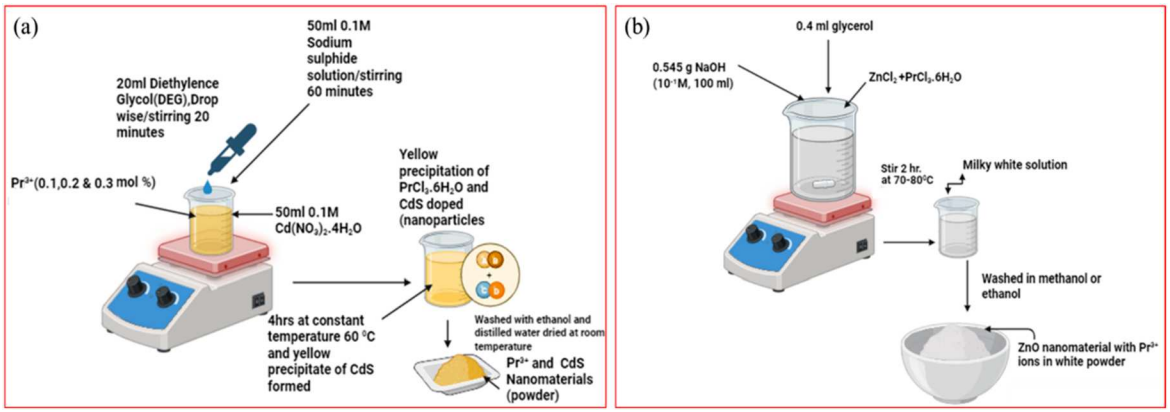

Figure 1. Synthesis mechanism of (a) Pr^{3+}-doped CdS and (b) Pr^{3+}-doped ZnO NPs.

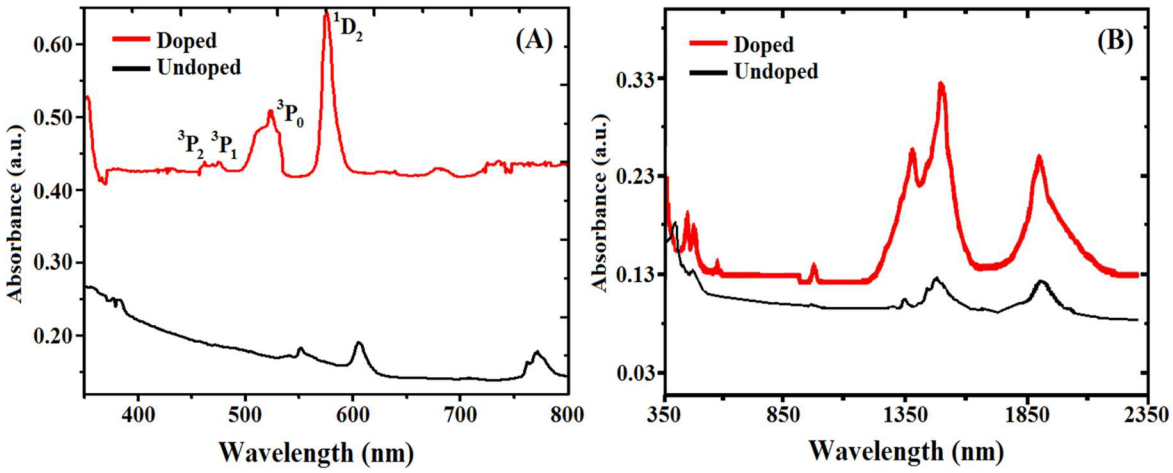

Figure 2. Absorption spectrum of (A) CdS: Pr^{3+} and (B) ZnO:Pr^{3+}NPs.

($\lambda = 0.15418$ Å), operated at 45 kV and 40 mA. Data were collected with a step size of 0.50° and a counting time of 1 s per step. Diffraction from various atomic planes generates a pattern that reveals information about the atomic arrangement within the crystal. The diffracted intensities were measured over a 2θ range of 10° to 80°. XRD analysis was conducted to determine the material's crystallinity, phase composition, lattice parameters, and any structural changes induced by doping. The micro-structural properties were analyzed using a scanning electron microscope (SEM) by FEI Quanta 200 F and a transmission electron microscope (TEM) by FEI Tecnai^{TM}G^2 20 S-twin.

Theoretical Consideration

Slater-Condon parameter.—Slightly different approaches have been utilized to calculate the electrostatic energy E_e[13–15] given as:

$$E_e = \sum_{k=2,4,6} f_k F^k \qquad [1]$$

where k is even and f_k is the coefficient of the linear combination of $4f$ radial functions and stand for the angular division of the relations. F^k is known as direct integral and are essentially a positive and lessening function of k, and are agreed by

$$F^k = \int_0^\infty \int_0^\infty \frac{r^k<}{r^{k+1}>} R_i^2(r_i) R_j^2(r_j) r_i^2 r_j^2 dr_i dr_j \qquad [2]$$

where R is the $4f$ radial wave function and i and j keep in touch correspondingly to the ith and $j$jh electrons under contemplation.[16] In sort to avoid large denominators appearing in the matrix basics calculation, a reduced Slater integral F_k can be introduced as:

$$F_k = \frac{F^k}{D_k} \qquad [3]$$

where D_k is the denominator, whose standards have been tabulated by Nielson and Coster.[17] Thus reduced Slater integrals can be represented as:

$$F_k = \frac{1}{D_k} \int_0^\infty \int_0^\infty \frac{r^k<}{r^{k+1}>} R_i^2(r_i) R_j^2(r_j) r_i^2 r_j^2 dr_i dr_j \qquad [4]$$

These F_2, F_4 and F_6 are known as Slater-Condon parameters.[18] F_k parametersare fundamental constants used to describe the electron-electron repulsion within an atom or ion, particularly among electrons in the same shell, such as the $4f$ electrons in RE ions.

Racah parameter.—Racah[13–15] has introduced electrostatic energy E_e as:

$$E_e = \sum_{k=1}^{3} e_k E^k \qquad [5]$$

where e_k is expectation values of the innovative operator and E^k represent the Racah parameters. The Racah parameters are empirical constants used in spectroscopy and coordination chemistry to describe the electron-electron repulsion within partially filled d- or f-orbitals of RE complexes. They quantify the inter-electronic

Table I. Experimental value of wavelength (λ), energy (Eexp) and oscillator strength (Pexp) for various absorption levels of 0.1 mol% Pr3+ doped CdS and ZnONPs.

Sample	Absorption levels	Wavelength λ (nm)	Wave number (1/λ) cm (E_{exp})	Oscillator strength ($P_{exp}\times10^{-6}$)
CdS:Pr^{3+}	$^3H_4\rightarrow{}^3F_2$	2015	4962	182.6
	$^3F_3$	1596	6265	304.7
	$^3F_4$	1465	6825	26.70
	$^1G_4$	975	10256	56.15
	$^1D_2$	576	17361	44.72
	$^3P_0$	523	19120	34.19
	$^3P_1$	465	21505	27.57
	$^3P_2$	423	23640	22.13
ZnO:Pr^{3+}	$^3H_4\rightarrow{}^3F_2$	4889	4809.18	79.82
	$^3F_3$	6246	6085.97	160.03
	$^3F_4$	6734	6737.69	−3.69
	$^1G_4$	9389	9824.61	−435.61
	$^1D_2$	17182	17121.62	60.38
	$^3P_0$	20661	20721.62	60.38
	$^3P_1$	21052	21232.58	−180.58
	$^3P_2$	22371	22415.73	−44.72

repulsion energy between electrons in the same shell and help in interpreting the electronic spectra of such complexes.

Lande' parameter.—The Hamiltonian due to spin–orbit interaction is given[19] by:

$$H_{S-O}=\sum_{i=1}^{n}\xi_i(r_i)(\vec{s_i}.\vec{l_i}) \quad [6]$$

where r_i, s_i, l_i are radial co-ordinates, spin angular momentum and orbital angular momentum of ith electron. The integral of ξ_i over the $4f$ radial wave function (R) is expressed[19] by

$$\zeta_{4f}=\int_0^{\infty}R_{4f}^2\,\xi(r_i)dr_i \quad [7]$$

is recognized as Lande' parameter. It plays a key role in determining the magnetic moments and magnetic susceptibility, especially in paramagnetic RE(trivalent lanthanide) compounds.

Nephelauxetic ratio.—In the case of lanthanide ions, the metal $4f$ orbital enlarge to a lesser degree. This is quantitatively measured in terms of nephelauxetic ratio (β') given as:

$$\beta'=\frac{F_k^g}{F_k^f} \quad [8]$$

Here g and f refer to complex and free ions. β' is used to quantify the reduction in inte-relectronic repulsion within the $4f$ orbitals when the ion forms a complex with ligands. However, due to the shielded nature of $4f$ orbitals, this effect is much weaker in RE ions compared to transition metals.

Bonding parameter.—Bonding parameter ($b^{1/2}$)quantifies the degree of covalency in the bond between a metal ion and its surrounding ligands in a complex. It is especially useful in the study of RE (lanthanide) and transition metal complexes. $b^{1/2}$ can be introduced in terms of β', as:[20]

$$b^{1/2}=\left[\frac{1-\beta'}{2}\right]^{1/2} \quad [9]$$

A real value of $b^{1/2}$ indicates covalent bonding.

Results and Discussion

Absorption spectra analysis.—The UV-visible spectroscopy is the interaction of radiation for the visible spectra ranging 300–1100 nm. The absorption spectra of 0.1 mol% Pr^{3+} doped CdS:Pr^{3+} and ZnO:Pr^{3+} NPs were recorded for the wavelength range 350–800 nm and 350–2350 nm, respectively, corresponding to metal transitions from ground level to excited levels. These spectra of Pr^{3+} doped CdS and ZnONPs are presented in Figs. 2A and 2B in terms of wavelength (nm) vs. absorbance (a.u.). The absorption bands' peak values in terms of λ (nm) and $E_{exp}(cm^{-1})$, along with the corresponding oscillator strength (P_{exp}) and assignments, are given in Table I for both CdS:Pr^{3+} and ZnO:Pr^{3+} NPs. Pr^{3+} doping introduces localized $4f$ states in CdS and ZnO, which modify their band structures and optical transitions. In CdS:Pr^{3+}, these states enhance photoluminescence and radiative recombination, while in ZnO:Pr^{3+} they generate sharp intra-$4f$ emissions and suppress deep-level defects. Thus, Pr^{3+} ions effectively tailor the luminescence efficiency and spectral response of both hosts. Eight absorption bands have been observed from the ground state $^3H_4$ to excited states $^3F_2$, $^3F_3$, $^3F_4$, $^1G_4$, $^1D_2$, $^3P_0$, $^3P_1$ and $^3P_2$ for 0.1 mol%Pr^{3+} doped CdS and ZnONPs. The experimental and calculated energy band positions

Table II. Experimental energy (E_{exp}), calculated energy (E_{cal}) and their differences (ΔE) for various absorption levels of 0.1 mol%, 0.2 mol% and 0.3 mol%Pr^{3+} doped CdS and ZnONPs.

		Pr^{3+} ion doping in CdS				Pr^{3+} ion doping in ZnO		
Parameters	Free CdS Ions	0.1 mol%	0.2 mol%	0.3 mol%	Free ZnO Ions	0.1 mol%	0.2 mol%	0.3 mol%
F_2 (cm^{-1})	305	332.21	331.80	331.60	322.09	316.5054	313.33	309.87
F_4 (cm^{-1})	51.88	47.47	46.55	47.22	44.46	43.69	43.25	42.77
F_6 (cm^{-1})	5.32	5.24	5.17	5.45	4.86	4.78	4.73	4.68
ζ_{4f}(cm^{-1})	730.5	979.38	998.78	980.61	741.00	731.07	708.16	736.73
E^1 (cm^{-1})	4728.9	4968.1	4926	5004.02	4728.92	4646.86	4600.34	4549.57
E^2 (cm^{-1})	24.45	25.16	25.37	25.34	24.75	24.30	24.06	23.79
E^3 (cm^{-1})	478.10	489.64	489.2	481.74	478.10	469.82	465.11	459.98
F_4/F_2	0.14	0.1428	0.140	0.142	0.14	0.138	0.138	0.138
F_6/F_2	0.02	0.0157	0.015	0.016	0.02	0.0151	0.0151	0.0151
E^1/E^3	9.89	10.14	10.07	10.38	9.89	9.89	9.89	9.89
E^2/E^3	0.05	0.051	0.051	0.052	0.05	0.05	0.0531	0.05
β'	–	1.00317	1.0019	1.0013	–	0.982	0.972	0.962
$b_{1/2}$	–	0.039	0.031	0.025	–	0.110	0.116	0.13

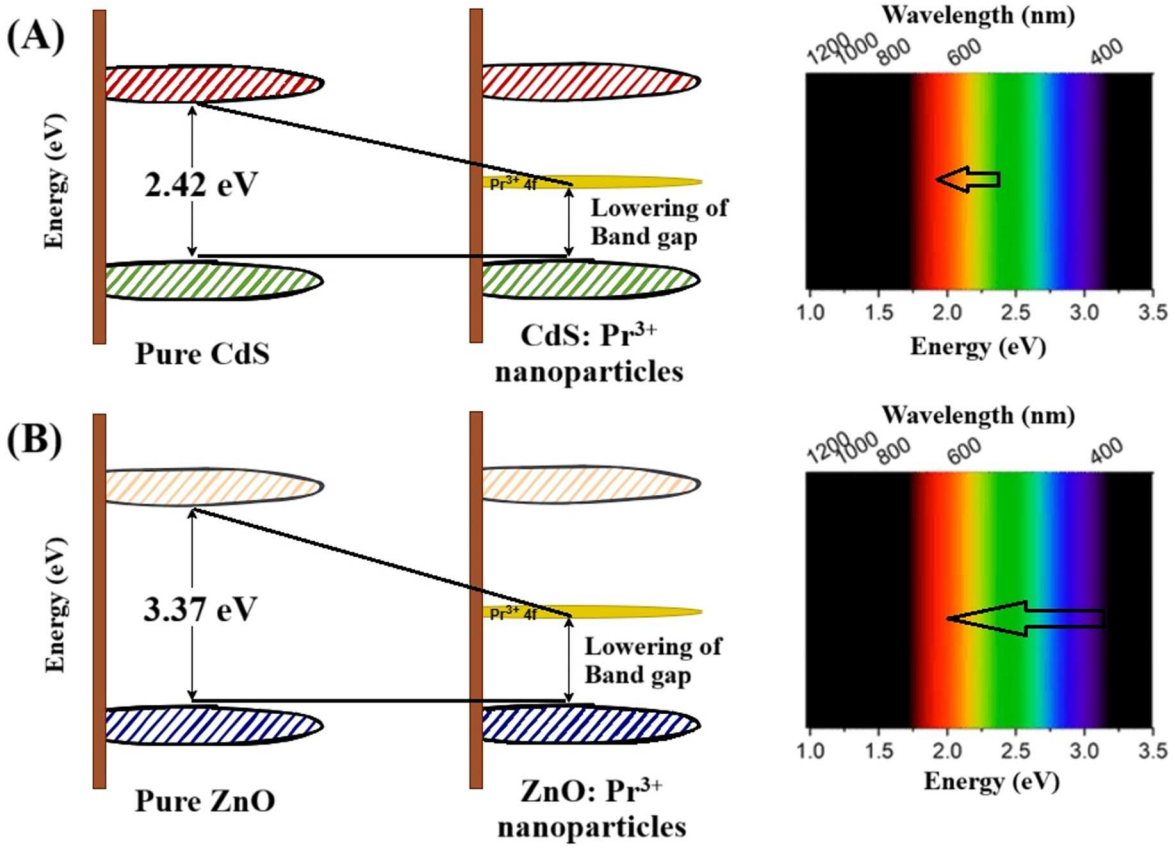

Figure 3. Proposed band diagram of (A) pure CdS and Pr^{3+}-doped CdS and (B) pure ZnO and Pr^{3+}-doped ZnO. Incorporation of Pr^{3+} introduces an intermediate energy level within the bandgap of the CdS/ZnO nanoparticles, effectively narrowing the bandgap of the pure material.

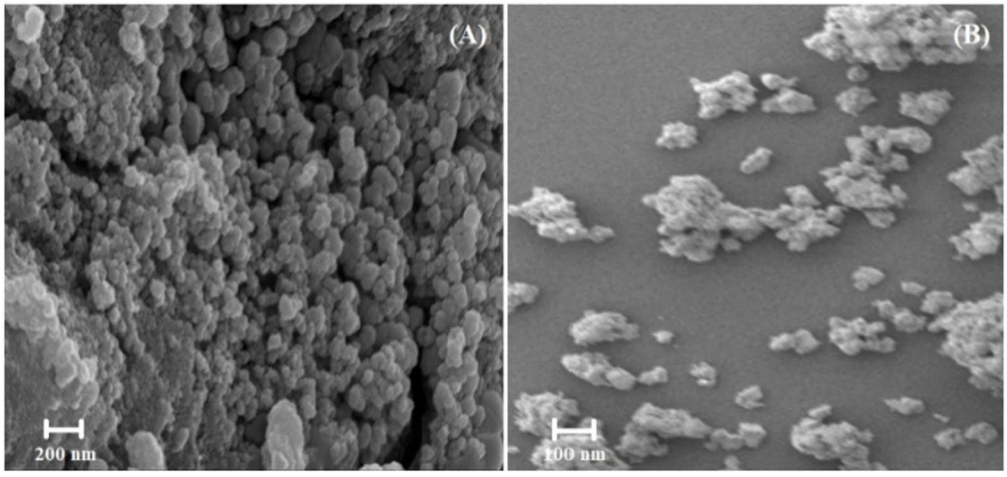

Figure 4. Typical SEM micrograph of (A) CdS: Pr^{3+} and (B) ZnO:Pr^{3+}NPs.

for 0.1 mol%, 0.2 mol% and 0.3 mol% of Pr^{3+} doped CdS and ZnONPs are given in Table II.

The discrepancy between the reported band gaps of bulk CdS (2.42 eV) and ZnO (~3.37 eV) and the observed absorption extending into the red and near-IR regions in Pr^{3+}-doped CdS and ZnO nanoparticles can be explained by several factors. Quantum confinement significantly affects the band structure in nanoparticles, with smaller sizes leading to widened band gaps and blue-shifted absorption, as observed in CdS nanoparticles.[21] However, Pr^{3+} doping introduces localized 4*f* energy levels within the band gap, which enable sub-band gap transitions and cause red shifts in absorption, depending on the doping concentration and the successful incorporation of Pr^{3+} into the crystal lattice.

As the concentration of Pr^{3+} increases, the bandgap shifts toward the visible region of the electromagnetic spectrum. This results in a red-shift in optical absorbance to longer wavelengths. Proposed band diagram of pure CdS/ZnO and Pr^{3+}-doped CdS/ZnOis shown in Fig. 3.

In both CdS and ZnO systems, the presence of Pr^{3+} can also induce crystal field splitting of 4*f* levels,[22] enabling intra-4f or charge transfer transitions in the visible to near-IR range. Additionally, dopant-induced defect states such as oxygen or sulfur

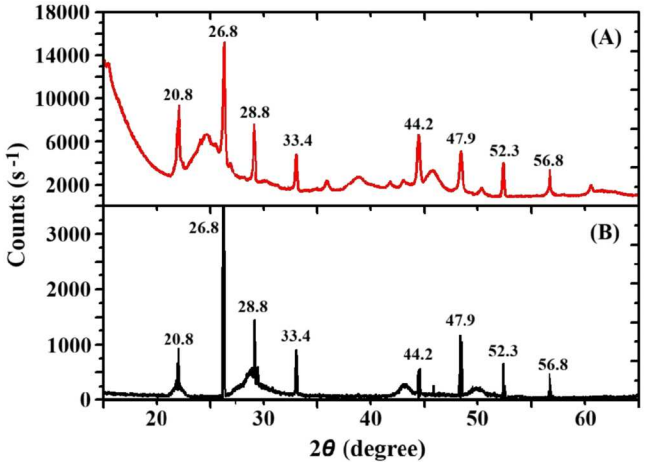

Figure 5. XRD spectra of (A) CdS NPs doped with 0.1 mol% of Pr^{3+} ion and (B) pure CdS NPs.

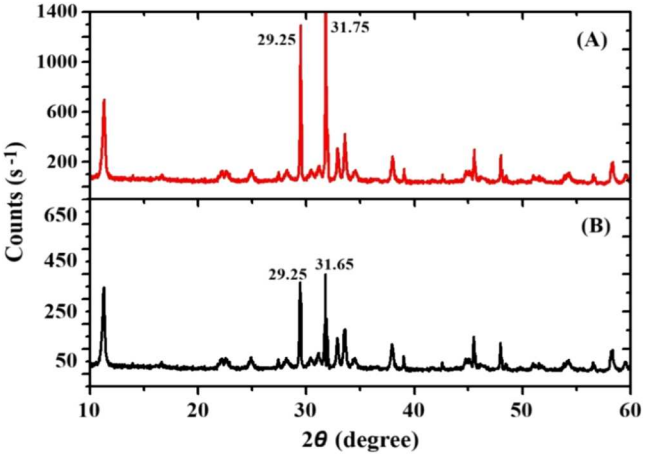

Figure 6. XRD spectra of (A) ZnO NPs doped with 0.1 mol% of Pr^{3+} ion and (B) pure ZnO NPs.

vacancies contribute further to the extended absorption. The interplay of these factors like quantum confinement, dopant levels, defect states, and crystal field effects explains the observed shifts in absorption and confirms the tunable nature of the optical properties in Pr^{3+}-doped CdS and ZnO nanoparticles.

Scanning electron microscopy (SEM).—Scanning electron microscopy (SEM) was obtained using FEI Quanta 200 F. A representative SEM image of 0.1 mol% Pr^{3+} ion doped CdSNPs [Fig. 4A], at ambient temperature, indicates an approximate spherical morphology of the CdSNPs, with sizes ranging from 1μm to 200 nm. In contrast, the SEM image of 0.1 mol% Pr^{3+} ion-doped ZnONPs [Fig. 4B], at room temperature, displays a variety of non-uniform, clustered structures of differing sizes, with an average size estimated to be between 200 nm and 20 nm. These particles exhibit distinct necking with adjacent particles. Due to the pronounced agglomeration observed in SEM, these dimensions represent apparent aggregate sizes rather than primary CdS:Pr^{3+}/ZnO:Pr^{3+} NPs. The true crystallite size was determined from XRD and further supported by TEM measurements, while SEM primarily provides information on aggregate morphology.

X-ray diffraction (XRD).—Figure 5 depicts the XRD spectra of the synthesized CdS: Pr^{3+} NPs and themost significant peaks are observed at approximately $2\theta = 26.8°$, 28.8°, 33.4°, 44.2°, 47.9°, 52.3°, and 56.8° correspond to characteristic reflections of the hexagonal crystal structure of CdS (JCPDS file no. 41–1049). These prominent diffraction peaks confirm the crystalline nature of CdSNPs. The presence of sharp and intense peaks, notably the most pronounced peak at 26.8°, indicates a well-ordered crystal lattice structure. The absence of significant impurity peaks further supports the synthesis purity and effective doping of Pr^{3+} ions in the CdS matrix. Figure 6 represents the XRD pattern of ZnO:Pr^{3+} NPs, displaying a dominant peak at around $2\theta = 31.75°$, which corresponds to the (100) crystal plane of wurtzite ZnO (JCPDS file no. 36–1451). The presence of other significant, sharp diffraction peaks also suggests highly crystalline wurtzite structure of ZnO NPs. The intensity and sharpness of peaks indicate good crystallinity and controlled particle growth during the synthesis. Both XRD patterns are typical for nano-structured materials, indicating successful doping and synthesis processes, with diffraction patterns aligning well with standard references. The incorporation of Pr^{3+} ions appears not to significantly distort the crystal lattice of CdS, while ZnO maintains its distinct wurtzite structure. Considering the peak at θ degree, average particle size has been estimated by Debye–Scherrer formula:[23]

$$D = 0.9\lambda/(\beta cos\theta) \quad [10]$$

The analysis of powder XRD pattern at room temperature shows that the sample formed is single phase with the spherical symmetry and average crystalline size of CdS: Pr^{3+} is lying in the range of 29.81–31.52 nm and the average crystalline size of ZnO: Pr^{3+} is lying in the range of 21.82–24.41 nm.

EDAX.—Representative energy dispersive X-ray (EDAX) spectra of CdS:Pr^{3+} and ZnO:Pr^{3+} NPs are shown in Figs. 7A and 7B, respectively. These spectra confirm the chemical composition of the NPs, clearly indicating the presence of Cd, S, and Pr in CdS:Pr^{3+}, and Zn, O, and Pr in ZnO:Pr^{3+}.

Transmission electron microscopy (TEM).—TEM was obtained using model FEI Tecnai^{TM}G^2 20 S-twin. TEM images of 0.1 mol% Pr^{3+} ion-doped CdS and ZnONPs are presented in Figs. 8A and 8B.

The right panel of the figure displays high-resolution TEM images that depict the Selected Area Electron Diffraction (SAED) pattern. The nearly spherical shapes of the dark spots in Fig. 8A suggest that the CdSNPs are predominantly spherical, whereas the nearly hexagonal shapes of the dark spots in Fig. 8B indicate that the ZnONPs are primarily hexagonal.

Spectroscopic analysis of energy interaction parameters.—The UV-Visible spectral regions, formed by energy transitions, involve the outer orbital or valence electrons. The spectra in liquid media are generally broad and relatively featureless, which indicates a blue shift absorption. UV-visible spectrophotometer used for primary application in quantitative analysis and calculates different parameters. The CdS doped with RE ions then has an increasing concentration and reduction of particle size. The optical properties of CdS/ZnONPs are highly size-dependent due to quantum confinement, where smaller particles exhibit increased band gaps and blue-shifted absorption. This effect becomes significant near the exciton Bohr radius and is influenced by synthesis conditions. Pr^{3+} doping further modifies optical behavior by introducing localized $4f$ states within the band gap, enabling new transitions and affecting photoluminescence. It also alters crystallite growth, morphology, and defect formation, impacting excitonic behavior. Thus, both reduced particle size and Pr^{3+} doping contribute to deviations from bulk optical properties through a combination of quantum and electronic effects. The RE ions have $4f^n$ configuration. The study of the energy level structure of RE ions (Pr^{3+}) is necessary for the interpretation of spectra. The absorption spectra of RE ions in the visible consist of narrow, weak bands. Using the measured band energies, the values of the Slater-Condon parameter (F_k), the Racah parameter (E^k), the Lande parameter (ζ_{4f}), the bonding parameter ($b_{1/2}$), and the Nephelauxetic ratio(β') have been calculated. The partial regression method determines the values of the partial derivatives and zero-order energies (E_{0j}).[24] The E_{0j} and partial derivatives of the energy levels have been given in Table II for CdS: Pr^{3+} and ZnO: Pr^{3+} NPs,

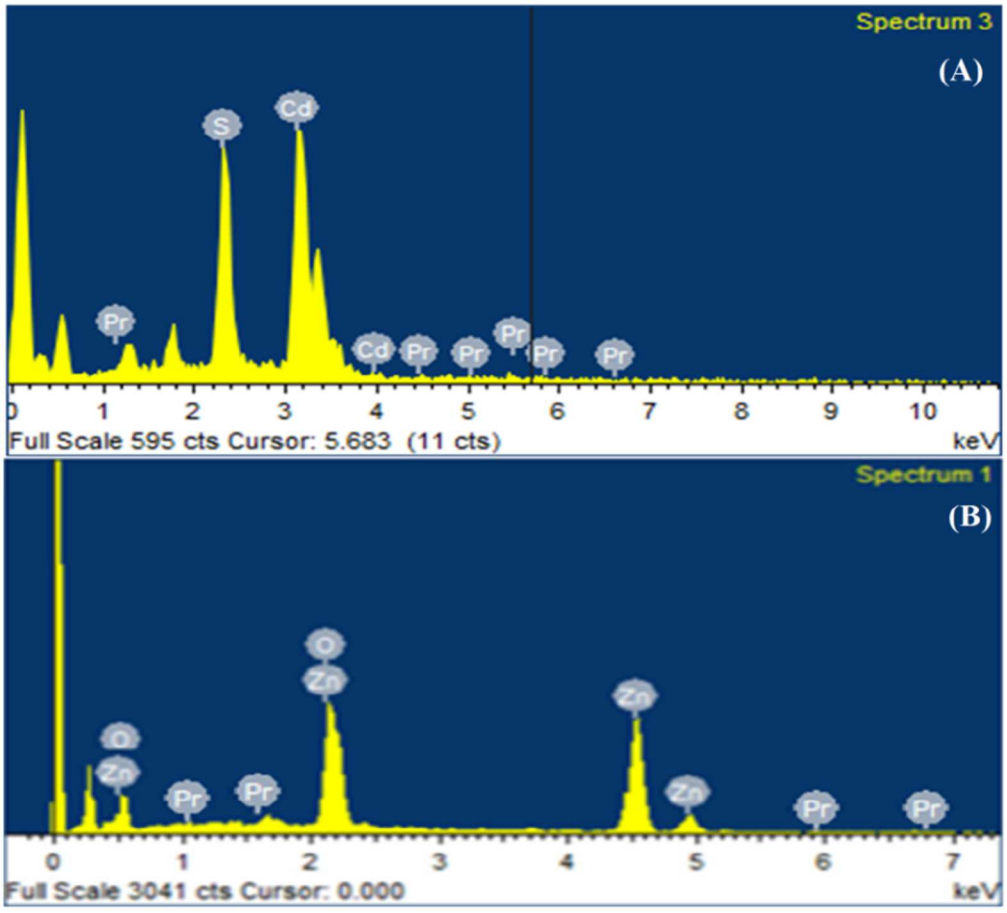

Figure 7. Representative EDAX spectra of (A) CdS:Pr^{3+} and (B) ZnO:Pr^{3+}NPs.

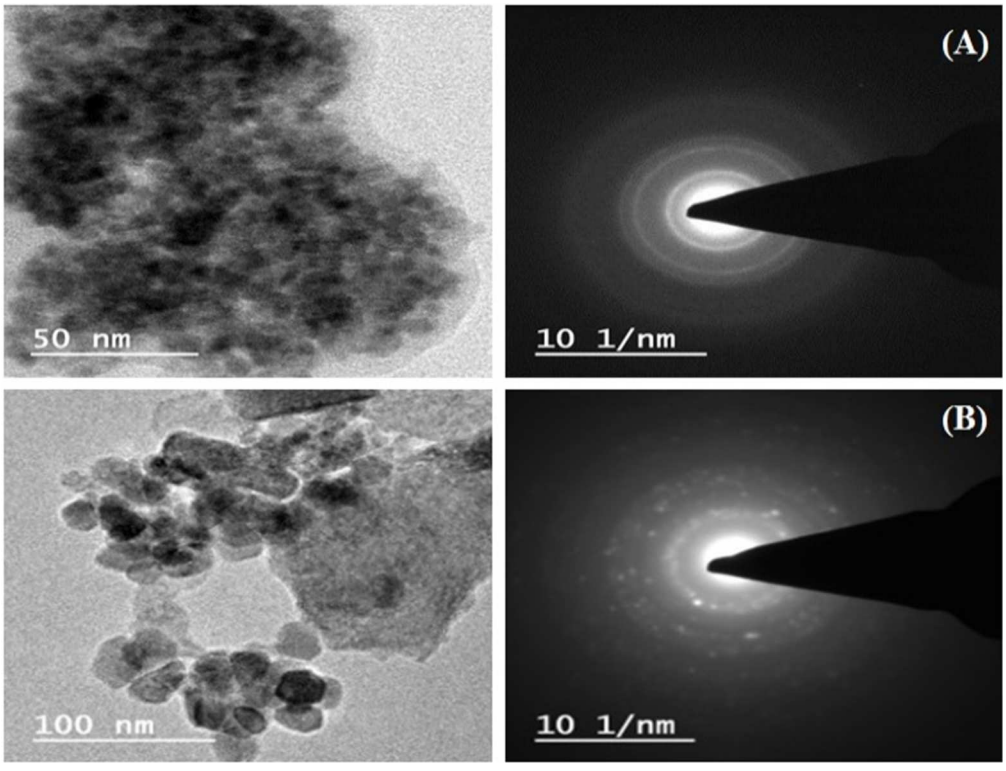

Figure 8. Typical TEM micrograph of (A) CdS: Pr^{3+} and (B) ZnO:Pr^{3+}NPs.

respectively. The CdS:Pr^{3+} and ZnO:Pr^{3+} NPs, the relation among different F_k parameters is found as $F_2 > F_4 > F_6$.

It is found that in CdS:Pr^{3+} NPs $F_4/F_2 \sim 0.140$–0.143 and $F_6/F_2 \sim 0.015$–0.016, while in ZnO:Pr^{3+} NPs $F_4/F_2 \sim 0.138$ and $F_6/F_2 \sim 0.015$, and are nearly the same as calculated considering radial eigen function to be hydrogenic. The F_k parameters are deduced from the E^k parameters are computed. Over the wide range of Pr^{3+} doping concentrations, the ratios of E^1/E^3 and E^2/E^3 are found to stay nearly constant and to be in good approximation with the corresponding hydrogenic ratios. This suggests that equivalent force fields are applied to Pr^{3+} ions at various doping concentrations.

Conclusions

The XRD analysis verified the structural properties of CdS:Pr^{3+} and ZnO:Pr^{3+} NPs. The SEM images confirmed the dimensions and morphology of the synthesized CdS:Pr^{3+} and ZnO:Pr^{3+} NPs. The nearly spherical and hexagonal shapes depicted in the TEM images indicate that the CdS and ZnONPs primarily display spherical and hexagonal shapes, respectively. All of the produced materials' absorption spectra, showed a considerable blue shift (472–504 nm) from the bulk CdS (525 nm) and ZnO (578 nm). However, in relation to the doping doses, doped materials' absorption spectra showed a red shift (414–550 nm).These may be attributed to quantum confinement effects, interfacial band alignment, and defect-induced states. The incorporation of Pr^{3+} introduces localized 4*f* levels within the band gap, facilitating additional sub-band gap transitions and effectively modifying the optical properties of the system. It is significant to note that the computed values of F_4/F_2 and F_6/F_2 are almost identical to the actual values when the radial eigenfunction is assumed to be hydrogenic. The ratios of E^1/E^3 and E^2/E^3 are found to remain almost constant over the entire range of Pr^{3+} doping concentrations. The interplay between quantum confinement and Pr^{3+} doping in CdS/ZnO nanocomposites offers an effective route to tailor their optical and electronic properties. Nanoscale effects, defect states, and localized 4*f* levels from Pr^{3+} ions contribute to a red shift in the absorption edge and enable sub-band gap transitions. These changes enhance control over absorption, emission, and band gap behavior, making the materials suitable for optoelectronic applications such as fiber-optic communication, display technologies, and X-ray imaging. Electrochemical analysis of doped and undoped samples further confirms the improved performance, highlighting their potential for next-generation photonic and electronic devices.

Acknowledgments

Authors are grateful to Institute Instrumentation Centre (IIC), IIT Roorkee, for providing facilities to perform TEM, SEM, XRD and absorption spectra studies of the sample. We are thankful to Prof. Ramesh Chandra, Head, IIC, IIT Roorkee for his valuable support in this study.

Authors Contribution

Jitender Pal Singh: Conceptualization and Methodology. Y.K. Sharma & Sudha Pal: Original draft writing. Atanu Nag & Naveen Kumar: Formal Analysis. Gulshan Dhillon & Jyoti Sahu: Investigation.

Funding

For this work, no funding was received from any governmental or non-profit organization.

Availability of Data

Data will be made available on reasonable request.

ORCID

Jitendra Pal Singh https://orcid.org/0000-0002-6328-7227
Sudha Pal https://orcid.org/0000-0002-1282-9663
Yogesh Kumar Sharma https://orcid.org/0000-0002-4324-9995
Atanu Nag https://orcid.org/0000-0003-0561-1946
Gulshan Dhillon https://orcid.org/0000-0001-9293-4369
Naveen Kumar https://orcid.org/0000-0001-8585-9372
Jyoti Sahu https://orcid.org/0000-0003-0485-6298

References

1. M. Nasrollahzadeh, S. Mohammad Sajadi, M. Sajjadi, and Z. Issaabadi, *Chapter 1 - An Introduction to Nanotechnology*, ed. M. Nasrollahzadeh et al. (Interface Science and Tech. Elsevier, Iran) 28, 27 (2019).
2. T. Jüstel, H. Nikol, and C. Ronda, "New developments in the field of luminescent materials for lighting and displays." *Angew. Chem. Int. Ed. Engl.*, **37**, 3084 (1998).
3. D. B. Barber, C. R. Pollock, L. L. Beecroft, and C. K. Ober, "Amplification by optical composites." *Opt. Lett.*, **22**, 1247 (1997).
4. G. Tessitore, G. A. Mandl, S. L. Maurizio, M. Kaur, and J. A. Capobianco, "The role of lanthanide luminescence in advancing technology." *RSC Adv.*, **13**, 17787 (2023).
5. C. K. Sheng and Y. M. Alrababah, "Thermal annealing gradient tailoring on ammonium nitrate-capped CdS nanospheres synthesized via green precipitation." *Heliyon.*, **10**, e30441 (2024).
6. Z. L. Wang, "Nanostructures of zinc oxide." *Mater. Today*, **7**, 26 (2004).
7. L. Schmidt-Mende and J. L. MacManus-Driscoll, "ZnO—nanostructures, defects, and devices." *Mater. Today*, **10**, 40 (2007).
8. Y. Li, C. Liao, and S. C. Tjong, "Recent advances in zinc oxide nanostructures with antimicrobial activities." *Int. J. Mol. Sci.*, **21**, 8836 (2020).
9. S. J. Pearton and F. Ren, "Advances in ZnO-based materials for light emitting diodes." *Current Opinion in Chemical Engineering.*, **3**, 51 (2014).
10. S. Raha and M. Ahmaruzzaman, "ZnO nanostructured materials and their potential applications: Progress, challenges and perspectives." *Nanoscale Adv.*, **4**, 1868 (2022).
11. P. Ilanchezhiyan, G. M. Kumar, M. Subramanian, and R. Jayavel, "Effect of Pr doping on the structural and optical properties of ZnO nanorods." *Materials Science and Engineering: B.*, **175**, 238 (2010).
12. G. Jose, V. Thomas, G. Jose, P. I. Paulose, and N. V. Unnikrishnan, "Application of a modified Judd–Ofelt theory to Pr^{3+} doped phosphate glasses and the evaluation of radiative properties." *J. Non-Cryst. Solids*, **319**, 89 (2003).
13. G. Racah, "Theory of complex spectra." *I. Phys.Rev.*, **61**, 186 (1942).
14. G. Racah, "Theory of complex spectra." *II. Phys.Rev.*, **62**, 438 (1942).
15. G. Racah, "Theory of complex spectra." *III. Phys.Rev.*, **63**, 367 (1942).
16. E. U. Condon and G. H. Shortley, *The Theory of Atomic Spectra* (Univ. Press, Cambridge) (1963).
17. C. W. Nielson and G. F. Koster, *Spectroscopic Coefficients for the p^N, d^N, and f^N Configurations* (MIT Press, Cambridge) (1963).
18. M. Liska, P. Pelikan, and L. T. Nagy, "Systematic determination of the Slater-Condon parameters of atoms and ions with $K(2)L(8)3s^m3p^n$ configurations." *Chem. Zvesti.*, **29**, 577 (1975).
19. E. H. Carlson and G. H. Dieke, *Spectroscopic Report. J. Chem. Phys.*, **34**, 1602 (1961).
20. D. E. Henrie and G. R. Choppin, "Environmental effects on f–f transitions. II. Hypersensitivity in some complexes of trivalent neodymium." *J.Chem. Phys.*, **49**, 477 (1968).
21. W. W. Yu, L. Qu, W. Guo, and X. Peng, "Experimental determination of the extinction coefficient of CdTe, CdSe, and CdS nanocrystals." *Chem. Mater.*, **15**, 2854 (2003).
22. F. A. Cotton and G. Wilkinson, *Advanced Inorganic Chemistry* (John Wiley & Sons Inc., USA) 6th Ed. ed. (1999).
23. S. Kumar and JK. Sharma, "Stable phase CdS nanoparticles for optoelectronics A study on surface morphology, structural and optical characterization." *Materials Science Poland*, **34**, 368–373 (2016).
24. J. Anjaiah, C. Laxmikanth, N. Veeraiah, and P. Kistaiah, "Luminescence properties of Pr^{3+} doped Li_2O-MO-B_2O_3 glasses." *J.Lumin.*, **161**, 147 (2015).